Dynamic performance analysis of permanent magnet contactor with a flux-weakening control strategy

Xianbing Wang, Heyun Lin, Shuhua Fang, Ping Jin, Junhua Wang et al.

Citation: J. Appl. Phys. **109**, 07E707 (2011); doi: 10.1063/1.3549554
View online: http://dx.doi.org/10.1063/1.3549554
View Table of Contents: http://jap.aip.org/resource/1/JAPIAU/v109/i7
Published by the American Institute of Physics.

Dynamic performance analysis of permanent magnet contactor with a flux-weakening control strategy

Xianbing Wang,[1,2] Heyun Lin,[1,a)] Shuhua Fang,[1] Ping Jin,[1] Junhua Wang,[3] and S. L. Ho[3]
[1]*School of Electrical Engineering, Southeast University, Nanjing 210096, China*
[2]*State Key Laboratory of Electrical Insulation and Power Equipment, Xi'an Jiaotong University, Xi'an 710048, China*
[3]*Department of Electrical Engineering, Hong Kong Polytechnic University, Kowloon, Hong Kong*

(Presented 18 November 2010; received 1 October 2010; accepted 9 November 2010; published online 8 April 2011)

A new flux-weakening control strategy for permanent magnet contactors is proposed. By matching the dynamic attraction force and the antiforce, the terminal velocity and collision energy of the movable iron in the closing process are significantly reduced. The movable iron displacement is estimated by detecting the closing voltage and current with the proposed control. A dynamic mathematical model is also established under four kinds of excitation scenarios. The attraction force and flux linkage are predicted by finite element method and the dynamics of the closing process is simulated using the 4th-order Runge-Kutta algorithm. Experiments are carried out on a 250A prototype with an intelligent control unit to verify the proposed control strategy. © *2011 American Institute of Physics*. [doi:10.1063/1.3549554]

I. INTRODUCTION

New applications and new operating principles of permanent magnets (PM) are extended to contactors. Most development efforts of energy-saving PM contactors focus on control circuit design, magnetic field and dynamic performance analysis.[1–3] To reduce the contact bounces which is the main critical component that undermines the performance of contactors, the control strategies of closing phase selection and displacement profile have been reported.[4,5] However, there are insufficient studies on how the PM attraction force is regulated in the closing course to ensure the dynamic attraction force and antiforce match well enough in order to prolong the PM contactor's lifetime.

The purpose of this paper is to employ a new flux-weakening control strategy for improving the dynamic performance of PM contactor so as to reduce the terminal velocity and collision energy of the movable iron.

II. CONTROL STRATEGY

Figure 1 shows the proposed flux-weakening control strategy, in which the closing process is divided into four stages, which are, namely, flux-strengthening phase I ($0 \le x < x_1$), freewheeling phase II after flux-strengthening is switched off ($x_1 \le x < x_2$), flux-weakening phase III ($x_2 \le x < x_3$) and freewheeling phase IV after flux-weakening is switched off ($x_3 \le x \le x_4$). In phase I, positive pulse-width-modulation (PWM) voltage U_1 is applied to the coil to control the collision speed of the movable and stationary contacts to reduce the first contact bounce. A negative modulation voltage U_2 is applied to the coil at the flux-weakening control displacement point ($x = x_2$) in the flux-weakening phase III. This generates a negative current in the coil to weaken the PM magnetic field so as to reduce the PM attraction force quickly toward the closing end to reduce the second contact bounce.

III. MAGNETIC FIELD ANALYSIS

Considering the structural symmetry of the proposed PM actuator,[3] only 1/4 of the volume is needed in the analysis. Neglecting both eddy current and hysteresis, the nonlinear magnetic field satisfies the following governing equations:

$$\begin{cases} \nabla \times \nu(\nabla \times \boldsymbol{A}) = \boldsymbol{J} & \text{in } \Omega_s \\ \nabla \times \nu(\nabla \times \boldsymbol{A} - \boldsymbol{B_r}) = 0 & \text{in } \Omega_m \end{cases} \tag{1}$$

where $\boldsymbol{J}$ is the current density of the exciting current, ν is the reluctivity, $\boldsymbol{A}$ is the magnetic vector potential, $\boldsymbol{B_r}$ is the residual flux density of PM.

Figure 2 gives the flux density distributions with the PM actuator at the flux-weakening control point ($x_2 = 13$ mm) under three different excitation conditions. It can be seen that the PM magnetic field is gradually weakened as the negative current increases.

Figure 3 shows the attraction force and antiforce versus displacement. When compared to the other two curves without any intelligent control strategy, it can be seen that the attraction force curve 3 of the proposed PM contactor under the flux-weakening control strategy matches better with the antiforce curve.

IV. DYNAMIC SIMULATION MODEL

A. Control circuit topology

Figure 4 shows the main circuit topology of the intelligent control unit. When both Q_1 and Q_3 are switched on, the

a)Author to whom correspondence should be addressed. Electronic mail: hyling@seu.edu.cn.

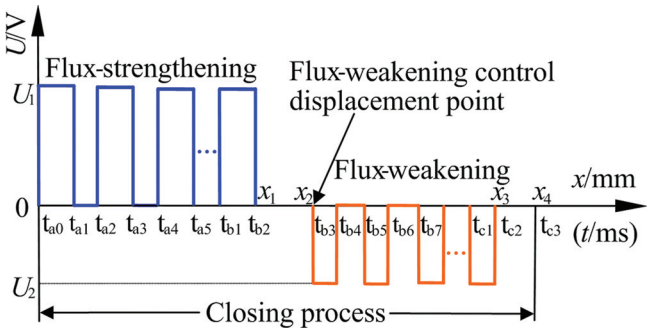

FIG. 1. (Color online) Flux-weakening control strategy.

coil generates a positive current to realize closing. When the flux-weakening control point is reached, both Q_1 and Q_3 are switched off and both Q_2 and Q_4 are switched on to generate a negative current in the coil to reduce the attraction force toward the closing end.

B. Movable iron displacement estimation

Figure 5 shows the equivalent magnetic circuit of the double E-core PM actuator. Due to structural symmetry of the actuator, Fig. 5(a) is simplified as Fig. 5(b).

As shown in Fig. 5, $\Re_m$ is the PM reluctance, $\Re_{di(i=1,2,3)}$ and $\Re_{sj(j=1,2,3)}$ are the respective reluctances of the movable and stationary iron middle column, yoke and the side column. $\Re_a$ and $\Re_g$ are the working air-gap reluctances of the middle and side column, respectively.

Considering the flux leakage by a coefficient of flux leakage k_σ, the flux produced by the PM in the movable iron can be expressed as

$$\varphi_{mm} = \varphi_{pm}/k_\sigma \tag{2}$$

where φ_{pm} is the total flux of the PM. By curve fitting, the coefficient of flux leakage can be approximately given by

$$k_\sigma = \frac{l_0 + h_m}{h_m} \tag{3}$$

where l_0 is the working air-gap length of the middle breaking position, h_m is the height of PM.

According to Fig. 5(b), by combining (2) and (3), the leakage magnetic reluctance is given by

$$\Re_l = \frac{2(\Re_{fe} + \Re_g/2)}{k_\sigma - 1} \tag{4}$$

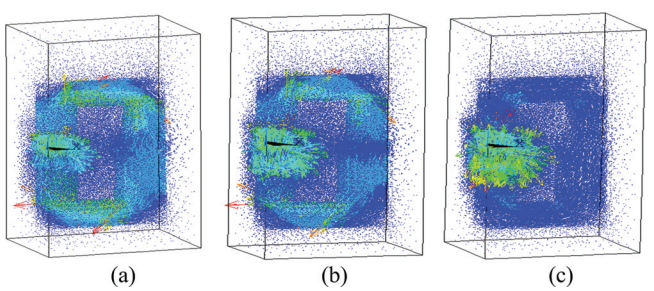

FIG. 2. (Color online) Flux density distributions. (a) PM only. (b) PM and i = −0.25A. (c) PM and i = −0.5A.

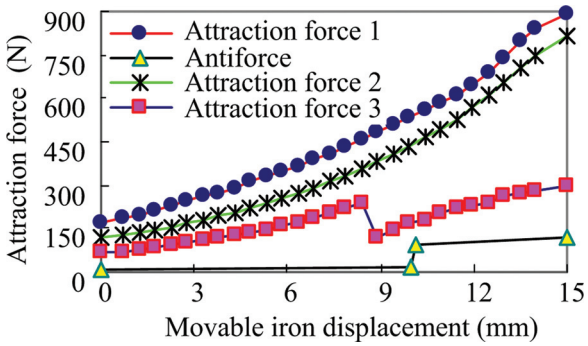

FIG. 3. (Color online) Attraction force and antiforce vs displacement.

where $\Re_{fe}$ is the total reluctances of ferromagnetic material. The total reluctance of the magnetic circuit is

$$\Re = \frac{1}{\mu_0 S}\left[\frac{l_g}{k_\sigma} + l_0 - \left(1 + \frac{1}{k_\sigma}\right)x + \frac{l_c}{\mu_{rm} k_\sigma}\right] + \Re_m \tag{5}$$

where l_g is the working air-gap length of the both sides, l_c is the total length of the closing magnetic circuit, μ_{rm} is the relative permeability of the ferromagnetic material.[5]

According to Ampere's law,

$$Ni + F_m = Hl_c + \varphi_{gap}\Re_{gap} \tag{6}$$

where F_m is the magnetomotive force (mmf) of the PM, N is the coil turns, φ_{gap} is the flux through the working air-gap, $\Re_{gap}$ is the reluctance of the working air-gap.

Substituting the working air-gap mmf $\varphi_{gap}\Re_{gap}$ with a constant C_r, the coil inductance L can be obtained as

$$L = \frac{N^2}{\Re} = \frac{SN^2}{\frac{l_g + k_\sigma l_0 - (k_\sigma + 1)x}{k_\sigma \mu_0} + \frac{l_c + b(Ni + F_m)}{ak_\sigma} + S\Re_m} + C_r \tag{7}$$

where a and b are the constants of the froëlich equation, S is the cross section area of the PM. Thus, the movable iron displacement x can be estimated by[5]

$$x = \frac{l_g + k_\sigma l_0}{k_\sigma + 1} - \frac{k_\sigma \mu_0 S}{k_\sigma + 1}\left(\frac{N^2 i}{\psi_0 + \int_0^t (u - iR)dt - C_r i} - \Re_m\right) + \frac{\mu_0[l_c + b(Ni + F_m)]}{a(k_\sigma + 1)} + \xi_c \tag{8}$$

where ξ_c is a modified constant to consider the air-gap fringing flux.

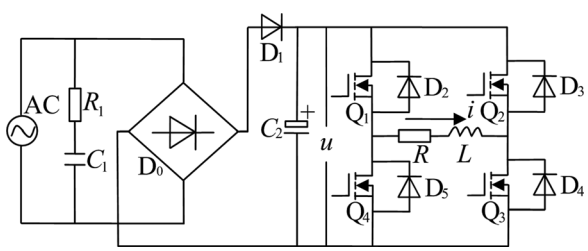

FIG. 4. Main circuit topology of the intelligent control unit.

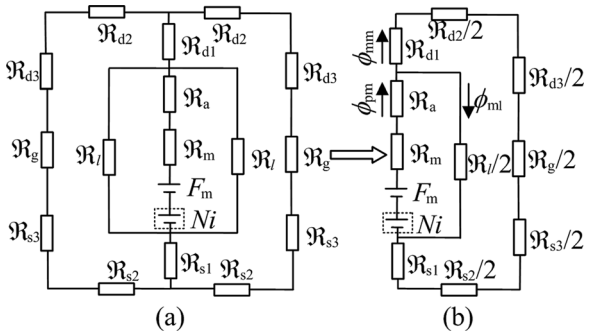

FIG. 5. Equivalent magnetic circuit.

C. Dynamic model

The PM contactor is a coupled system which satisfies the voltage equivalence and D'Alembert's mechanical motion equations simultaneously. The coil is driven by positive and negative PWM pulses during the closing process in which there are four working states, namely, flux-strengthening, freewheeling after flux-strengthening is switched off, flux-weakening and freewheeling after flux-weakening is switched off. The system under the four working states satisfies the same type of differential equation as follows:

$$\begin{cases} \frac{d\psi}{dt} = \pm u - i(\psi x)R \\ \frac{dv}{dt} = \frac{F(\psi,x)-F_f(x)}{m} \\ \frac{dx}{dt} = v \\ u|_{t=t_{a0}=0} = U_1, \quad u|_{t=t_{a1}=0} \\ \psi|_{t=t_{a0}=0} = \psi_0, \quad v|_{t=t_{a0}=0} = 0, \quad x|_{t=t_{a0}=0} = 0 \\ \psi|_{t=t_{a1}} = \psi_{t_{a1}}, \quad v|_{t=t_{a1}} = v_{t_{a1}}, \quad x|_{t=t_{a1}} = x_{t_{a1}} \\ \psi|_{t=t_{b2}} = \psi_{t_{b2}}, \quad v|_{t=t_{b2}} = v_{t_{b2}}, \quad x|_{t=t_{b2}} = x_{t_{b2}} \\ u|_{t=t_{b3}} = U_2, \quad u|_{t=t_{b4}} = 0 \\ \psi|_{t=t_{b3}} = \psi_{t_{b3}}, \quad v|_{t=t_{b3}} = v_{t_{b3}}, \quad x|_{t=t_{b3}} = x_{t_{b3}} \\ \psi|_{t=t_{b4}} = \psi_{t_{b4}}, \quad v|_{t=t_{b4}} = v_{t_{b4}}, \quad x|_{t=t_{b4}} = x_{t_{b4}} \\ \psi|_{t=t_{c2}} = \psi_{t_{c2}}, \quad v|_{t=t_{c2}} = v_{t_{c2}}, \quad x|_{t=t_{c2}} = x_{t_{c2}} \end{cases} \tag{9}$$

where v is the closing velocity, m is the mass of the motion parts, F is the dynamic attraction, F_f is the antiforce. The control voltage u is "+" under both flux-strengthening and flux-weakening states. Conversely, "−" is assumed under freewheeling state.

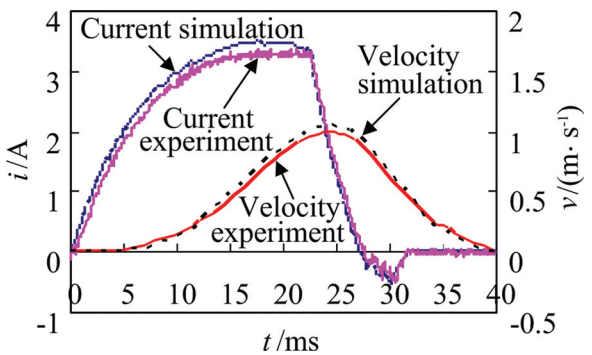

FIG. 6. (Color online) The simulated and experimental results of velocity and current.

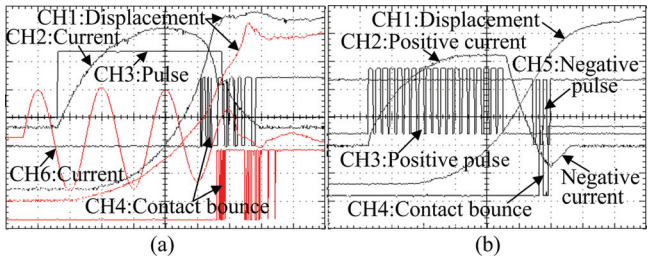

FIG. 7. (Color online) Experimental waveforms of three control schemes. (a) Without intelligent control in black lines and commercial contactor in red lines. (b) Flux-weakening control at $x_2 = 9$ mm (CH1: 500 mV/div corresponds to 2.5 mm/div; CH2: 100 mV/div corresponds to 1 A/div; CH3: 2 V/div; CH4: 2 V/div; CH5: 2 V/div; CH6: 200 mV/div corresponds to 2 A/div) (time scale: 5 ms/div for black lines; 10 ms/div for red lines).

The 4th-order Runge-Kutta method can be used to simulate the dynamic performance of the PM contactor during the closing process by coupling the electric circuit equation, magnetic field and motion equation together.

V. SIMULATION RESULTS AND EXPERIMENT

Figure 6 shows the simulated velocity of the movable iron and current curves as well as experimental waveforms during a complete closing process. It can be seen that the experimental results agree well with the simulated ones.

Figure 7 shows the experimental contact bounce waveforms of a PM contactor with and without flux-weakening control as well as that of a commercial contactor. It can be seen that soft landing of the movable iron can be realized in the proposed control. This is because the positive and negative currents in the coil are effectively controlled and the first and the second contact bounces are thus reduced significantly for the PM contactor with flux-weakening control when compared to the other two kinds of contactors.

VI. CONCLUSIONS

This paper reports a novel flux-weakening control strategy which has been successfully applied to a PM contactor to improve its dynamic performance and hence prolonging its electrical lifetime. Experimental results are shown to verify the proposed control strategy as being correct and effective for adjusting the PM magnetic field.

ACKNOWLEDGMENTS

This work was supported by the NSFC under Grant No. 50907007, the NSF of Jiangsu Province under Grant No. BK2010197, the HTRDP under Grant No. 2006AA05Z224 and the State Key Laboratory of Electrical Insulation and Power Equipment under Project No. EIPE10209.

[1]C. T. Chi, WSEAS Trans. on Electro. 5, 313, (2008).
[2]M. Z. Rong, J. Y. Lou, Y. Y. Liu, and J. Li, IEICE Trans. Electron. E89-C, 1210 (2006).
[3]S. H. Fang and H. Y. Lin, IEEE Trans. Magn. 45, 2990 (2009).
[4]C. T. Chi, Active and Passive Electronic Comp. 2009, 1 (2009).
[5]X. B. Wang, H. Y. Lin, and S. L. Ho, IEEE Trans. Magn. 46, 1633 (2010).